CHAOTIC DYNAMICS IN A SLOWLY ROTATING DRUM

DINÁMICA CAÓTICA EN UN TAMBOR GIRATORIO LENTO

H. Maghsoodi[a] and E. Luijten[a,b†]

a) Graduate Program in Applied Physics, Northwestern University, Evanston, Illinois 60208, U.S.A.
b) Departments of Materials Science & Engineering, Applied Mathematics and Physics & Astronomy, Northwestern University, Evanston, Illinois 60208, U.S.A; luijten@northwestern.edu†
† corresponding author

Recibido 19/3/2016; Aceptado 19/4/2016

Recent computational work (Banigan *et al.*, Nat. Phys. 9, 288 (2013)) has demonstrated that jamming and unjamming in a shear cell can be described in terms of chaotic dynamics. Experimental work (Wang *et al.*, Sci. Rep. 5, 8128 (2015)) found that avalanches in a rotating drum behave consistently with this description. We employ computer simulations to examine the chaotic dynamics accompanying granular avalanches in the rotating-drum system. These simulations directly evolve imposed perturbations and provide access to the largest short-time Lyapunov exponent. We find that the local chaotic properties of the system and its dynamics are indeed coupled; the system becomes chaotic as avalanches develop, and returns to a non-chaotic state as avalanches decay. Interestingly, the transition between chaotic and non-chaotic regimes lags behind the change in avalanche state. This contrasts with prior work on the shear cell, where the same force model yielded dynamics that becomes chaotic *leading up to*, rather than lagging behind, local reorganizations of disks.

Trabajo computacional reciente (Banigan y *col.*, Nat. Phys. 9, 288 (2013)) ha demostrado que el "jamming" y "unjamming" en una celda de cizalladura puede ser descrito en términos de dinámica caótica. Se ha encontrado experimentalmente (Wang y *col.*,Sci. Rep. 5, 8128 (2015)) que las avalanchas en un tabor rotatorio se comportan consistentemente con esta descripción. Utilizamos simulaciones computacionales para examinar la dinámica caótica que acompaña a las avalanchas granulares en el sistema de tambor rotatorio. Estas simulaciones involucran directamente perturbaciones impuestas, y permiten acceder al exponente más grande de Lyapunov de corto tiempo. Encontramos que las propiedades caóticas locales del sistema y su dinámica están, de hecho, acopladas; el sistema se vuelve caótico cuando se desarrollan las avalanchas, y retorna al estado no-caótico cuando éstas disminuyen. Resulta interesante que la transición entre los regímenes caótico y no-caótico va detrás del cambio del régimen de avalanchas. Esto contrasta con trabajos previos en la celda de cizalladura, donde el mismo modelo de fuerza resulta en una dinámica caótica que conduce, en vez de ser el resultado, a reorganizaciones locales de los discos.

PACS: 05.45.Pq Numerical simulations of chaotic systems, 45.70.Ht Avalanches, 45.70.Mg Granular flow: mixing, segregation and stratification, 05.45.-a Nonlinear dynamics and chaos

I INTRODUCTION

The ubiquity of granular materials—from pharmaceutical [1, 2] and semiconductor [1] industries to geology and astrophysics—has fueled over a century of research, mainly in industry-related communities [3,4]. Motivated by a desire to understand the physics of this complex class of materials, a wider theoretical perspective has emerged in the past few decades [5–9]. Of particular interest is the *jamming transition*, wherein a minute increase in the packing density drives a system from a liquid-like to a rigid state. This transition plays a central role in many promising new fields, including soft robotics and nanomanufacturing [10–12]. It also provides an ideal context for studying dissipative, non-equilibrium processes consequential to the understanding of life [13] and for fundamental research into non-equilibrium statistical mechanics [14, 15]. Yet, despite a flurry of research in the late 1990s and early 2000s following seminal work by Liu and Nagel [16], the jamming transition continues to elude a concrete, general explanation. In fact, studies have uncovered a splattering of different jamming regimes within a very narrow window of packing densities, including jammed [16], marginally jammed [17], shear-jammed [18], and fragile states [19] among others. This complexity makes a general, unifying perspective all the more desirable.

Recent computational work [20] has suggested that jamming may be understood more generally from an unexpected perspective. For a system of frictional disks in a two-dimensional (2D) shear cell a transition was observed from a chaotic to a non-chaotic state upon increase of the packing fraction. In the thermodynamic limit this transition, as characterized by a sign change of the largest global Lyapunov exponent, was found to coincide with the widely studied jamming transition of frictionless 2D disks [21]. Moreover, the largest *local* Lyapunov exponent $\lambda(t)$ was found to provide interesting information on the short-time dynamics of this system, temporarily becoming positive during the local reorganizations of disks. A corollary of this observation is that $\lambda(t)$ and its associated Lyapunov vector may be used as a predictive tool for such events [13,20], with potentially important applications ranging from geology to materials design [11].

This new perspective on the jamming transition, while promising both as a characterization tool and as a source of insight, must be explored for systems other than the 2D

shear cell. Here, we aim to extend the methods of Ref. [20] to avalanches in a 2D rotating drum. Slip events in a shear cell are analogous to the onset of avalanches in the rotating drum. Experimental quantification of chaotic properties during the jamming transition has proven to be particularly challenging for this system [22]. Thus, our work offers the additional benefit of guiding future experimental studies. By employing the same interaction model as Ref. [20] we test to which extent the connection between dynamic behavior and chaotic properties carries over to systems other than the 2D shear cell. We find that the observations for the shear cell indeed apply to a larger class of granular systems, but also observe remarkable differences.

II MODEL AND METHODS

II.1 Physical Model

We perform quasi-2D molecular dynamics (MD) simulations of a 1:1 bidisperse collection of cylindrical disks inside a rotating drum and subject to a gravitational field $\mathbf{g}$, following an experimental study [22]. Although physical disks will deform under the stress of contacts, for computational efficiency we treat our disks as rigid cylinders and employ a linear spring–dashpot model (Fig. 1) [23–25]. For two contacting disks i and j with respective diameters d_i and d_j, the force $\mathbf{f}_{ij}$ on disk i by disk j contains both tangential and normal components and is described by

$$\mathbf{f}_{ij} = \begin{cases} \mathbf{f}_{ij}^{\mathrm{n}} + \mathbf{f}_{ij}^{\mathrm{t}} = \left(-k_{\mathrm{n}}\delta\hat{\mathbf{r}}_{ij} - \gamma_{\mathrm{n}}\mathbf{v}_{ij}^{\mathrm{n}}\right) - \min\left(\gamma_{\mathrm{t}}v_{ij}^{\mathrm{t}}, \mu f_{ij}^{\mathrm{n}}\right)\hat{\mathbf{v}}_{ij}^{\mathrm{t}} & \delta \le 0 \\ 0 & \delta > 0 \end{cases} \quad (1)$$

where k_{n} is an elastic constant, γ_{n} and γ_{t} are normal and tangential viscous coefficients, $\mathbf{r}_{ij} \equiv r_{ij}\hat{\mathbf{r}}_{ij} = \mathbf{r}_i - \mathbf{r}_j$ is the vector from disk j to disk i, $\delta = r_{ij} - \frac{1}{2}\left(d_i + d_j\right)$ is the (negative) overlap distance, and $\mathbf{v}_{ij}$ is the relative velocity with normal component $\mathbf{v}_{ij}^{\mathrm{n}} = \mathbf{v}_{ij}\cdot\hat{\mathbf{r}}_{ij}$ and tangential component $\mathbf{v}_{ij}^{\mathrm{t}} \equiv v_{ij}^{\mathrm{t}}\hat{\mathbf{v}}_{ij}^{\mathrm{t}} = \mathbf{v}_{ij} - \mathbf{v}_{ij}^{\mathrm{n}}$. The simplest choice for the tangential frictional term would be Coulomb friction, $\mathbf{f}_{ij}^{\mathrm{t}} = -\mu f_{ij}^{\mathrm{n}}\hat{\mathbf{v}}_{ij}^{\mathrm{t}}$, but this results in an ill-defined force at $v_{ij}^{\mathrm{t}} = 0$ [26]. To circumvent the discontinuity of this force model, we introduce a dissipative frictional force which crosses over to Coulomb friction above a threshold value of v_{ij}^{t} determined by μ [23–26].

Since Eq. (1) is a contact force (*i.e.*, non-zero only when $\delta \le 0$), the net force on a disk i is $m_i\mathbf{g} + \sum_j \mathbf{f}_{ij}$, where the sum runs over all contacting disks j. We note that the parameters k_{n}, γ_{n}, and γ_{t} are material-dependent. Specifically, k_{n} and γ_{n} determine the stiffness of the material and its coefficient of restitution. However, γ_{t} is not derivable from material properties and must be chosen empirically [25]. The mass m_i of the disks is given by their effective height h. Table 1 summarizes the parameters used in our simulations to model a system of photoelastic disks [22–24].

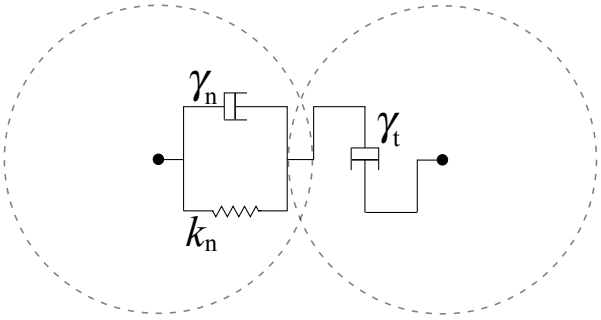

Figure 1. Linear spring–dashpot model for granular interactions. Two disks in contact experience a normal force that contains both elastic and dissipative contributions. The tangential (frictional) force is purely dissipative at small velocities and crosses over to Coulomb friction at larger velocities. See Eq. (1) of the main text.

Table 1. Physical parameters of the model in SI and reduced units. Reduced units are obtained by choosing the diameter and mass of a small disk as the unit length and mass, respectively, and adopting as energy unit the gain in potential energy of moving a small disk against gravity by a distance equal to its diameter.

Parameter	Symbol	SI units	Reduced units
Small disk diameter	d_{s}	1.2000×10^{-2} m	1
Large disk diameter	d_{l}	1.4000×10^{-2} m	1.1667
Wall disk diameter	d_{w}	1.6615×10^{-2} m	1.3846
Disk height	h	6.3500×10^{-3} m	0.52917
Drum diameter	d_{drum}	7.9339×10^{-1} m	66.115
Mass density	ρ	1060.0 kg/m^3	2.4061
Normal elastic coeff.	k_{n}	352.1 N/m	565.97
Normal viscous coeff.	γ_{n}	0.19 kg/s	8.7308
Tang. viscous coeff.	γ_{t}	0.15 kg/s	6.8927
Coeff. of friction	μ	0.44	-
Number of wall disks	n	150	-
Number of other disks	N	736	-

II.2 Simulation Method

We use the velocity-Verlet algorithm [27] to integrate our equations of motion. For computational efficiency, we construct pairwise Verlet neighbor lists [27] and take advantage of Newton's Third Law in computing the interparticle forces. To ensure that the step size Δt is sufficiently small, we choose Δt such that $\Delta t \le \tau/40$, where τ is the characteristic contact time between two disks [23]. Since $\mathbf{f}_{ij}^{\mathrm{n}}$ describes a damped harmonic oscillator with frequency $\omega = \sqrt{k_{\mathrm{n}}/m_{ij} - \gamma_{\mathrm{n}}^2/(4m_{ij}^2)}$, where $m_{ij} = m_i m_j/\left(m_i + m_j\right)$ is the effective mass, the contact time follows as $\tau = \pi/\omega$. The smallest value of τ occurs for contact between two small disks, and our choice $\Delta t = 4\times10^{-5}\ s$ yields $\Delta t \approx \tau/82$ for such contacts.

The drum is created by placing n wall disks on the vertices of a regular n-gon with side length d_{w} and is set into rotation with a fixed period $T = 900\ s$. We place the N non-wall disks randomly inside the drum and allow them to fall to the bottom due to the background gravitational field (Fig. 2(a)). Due to the drum's slow rotation rate and the lack of static friction in Eq. (1), we do not observe the build-up of large angles of inclination of the granular pile. Rather, once an

avalanche begins, it advances continuously as long as the drum rotates. To study both onset and decay of avalanches, we simulate these two regimes separately and for each we obtain averages over many runs. We compute the system's global speed $V(t) = \sqrt{\sum_i |\mathbf{v}_i(t)|^2}$ (where the sum runs over all disks and $\mathbf{v}_i(t)$ is the velocity of disk i at time t) at each time step to determine when an avalanche occurs. To study the avalanche *onset* (Fig. 2(b)), we begin collecting data after a brief equilibration period, corresponding to one degree of rotation, so before the avalanche has started. The onset is then defined as the point where $V(t)$ begins to increase (cf. Fig. 3 below). To simulate avalanche *decay* we first allow the drum to rotate long enough to ensure the production of a continuous avalanche. We then begin collecting data for 5 seconds before abruptly stopping the drum, triggering a decay in $V(t)$ (cf. Fig. 4). By our definition, this decay in $V(t)$ also marks the beginning of the avalanche decay.

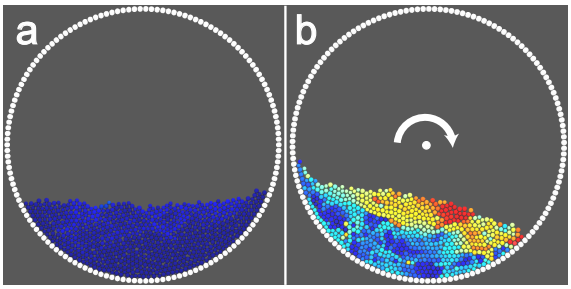

Figure 2. Snapshots from a simulation showing (a) the initial state of the system before the onset of an avalanche and (b) an avalanche resulting from the clockwise rotation of the drum. Disks are color-coded according to their speed, from blue (slow) to red (fast).

II.3 Quantifying Chaotic Dynamics

The chaoticity of a d-dimensional dynamical system may be quantified by a set of d Lyapunov vectors—which comprise an orthogonal set in phase space—and their corresponding exponents [28, 29]. Sorted by decreasing value, these exponents describe the exponential growth rates of perturbations along the directions in phase space described by the corresponding Lyapunov vectors. In this paper, we quantify the *locally* (*i.e.*, in the short term) most chaotic mode of our system via the first local Lyapunov vector $\mathbf{y}(t)$ and its corresponding local Lyapunov exponent $\lambda(t)$. We emphasize that these quantities are dynamics and describe only the short-time chaoticity of the system. The most unstable direction in phase space at one time is not necessarily so at future times, and $\lambda(t)$ is likewise subject to change [28, 29]. For a 2D system with N disks, we define a $4N$-dimensional perturbation vector $\boldsymbol{\delta}\mathbf{u}(t) \equiv (\{\boldsymbol{\delta}\mathbf{r}_i(t)\}, \{\boldsymbol{\delta}\mathbf{v}_i(t)\})$, which consists of two components describing positional perturbations δx_i and δy_i and two components describing velocity perturbations $\delta v_{x,i}$ and $\delta v_{y,i}$ for each disk i. From our equations of motion we derive a set of linearized tangent-space equations governing the evolution of the perturbation $\boldsymbol{\delta}\mathbf{u}(t)$. During the MD simulation, we integrate these equations in conjunction with the standard equations of motion for the disks, and thus simultaneously compute the real-space dynamics of the system and its chaotic properties. A detailed account of the numerical methods—as well as details of the analysis of *global* chaotic properties of granular systems—is provided in Ref. [30].

In general, a random initial perturbation quickly aligns with $\mathbf{y}(t)$, which also ensures that its growth rate converges to that of $\mathbf{y}(t)$ [28, 29]. We evolve $\boldsymbol{\delta}\mathbf{u}(t)$ and compute its exponential rate of growth (or decay) between successive time steps as $\lambda(t) = (1/\Delta t)\ln(|\boldsymbol{\delta}\mathbf{u}(t)|/|\boldsymbol{\delta}\mathbf{u}(t-\Delta t)|)$. The first (global) Lyapunov exponent would be obtained by taking the limit $\Delta t \to \infty$ [28]. By definition [28, 29], chaotic systems possess at least one positive Lyapunov exponent, whereas non-chaotic systems have only negative exponents.

We are interested in quantifying the *local*, rather than the global, chaoticity of our system, and we do so by computing $\lambda(t)$ during the evolution of an avalanche. For each run, we evolve a single perturbation vector, which is initialized by setting, on average, 10 percent of its components to non-zero values. Both the components and their values are chosen from a uniform random distribution. We compute the exponential growth rate of the perturbation vector at each time step. To focus on the chaotic properties of the disks that make up the contact network, at each time step we identify "rattler" disks with only zero or one contacts and exclude the corresponding components of the perturbation vector from growth-rate calculations during that step [30]. To achieve good statistics, we average over more than 70,000 pairs of avalanche onsets and decays, started from different random initial configurations.

III RESULTS AND DISCUSSION

We begin by investigating the evolution of $\lambda(t)$ during the onset of an avalanche. Even after averaging over many thousands of runs, $\lambda(t)$ exhibits a high level of noise (Fig. 3, blue points). This is to be expected since the dynamics near and along a chaotic attractor often varies quickly and dramatically [28, 29]. By taking the moving average

$$\overline{\lambda}(t) = \frac{1}{2q+1}\sum_{k=-q}^{q}\lambda(t+k\Delta t)\,, \tag{2}$$

with a narrow window $[t-q\Delta t, t+q\Delta t]$, we find that the data converge to a smoothly varying average behavior (Fig. 3, light blue dashed line). We choose a moving average width $(2q+1)\Delta t = 0.5$ s, but even a window five times narrower does not change the results appreciably. We also filter the original data using a low-pass filter (keeping only the lowest 0.008 percent of frequencies) and find that the resulting low-frequency modes of the data closely trace the moving-average behavior. The moving average $\overline{\lambda}(t)$ reveals a sign change as the avalanche progresses, in qualitative agreement with the observations in Ref. [20], where the non-avalanching regime is associated with a negative local Lyapunov exponent that crosses over to a positive value after the avalanche begins.

For a more quantitative analysis, we must determine the onset of the avalanche as well as the time at which $\overline{\lambda}(t)$

changes sign. Assuming a linear fit (Fig. 3, orange line segment) to $\lambda(t)$ for $10\,s < t < 20\,s$, we locate the sign change of the local Lyapunov exponent at $t = 14.5 \pm 0.2 s$. We note that this fit agrees both with $\overline{\lambda}(t)$ and with the low-pass filtered data of $\lambda(t)$ within the error of the fit. The global speed $V(t)$ exhibits non-monotonic behavior immediately after $t = 0$ s, due to decay of "start-up" effects of the rotation of the drum, followed by the onset of the avalanche. Fitting a quadratic time dependence to $V(t)$ for $1\,s < t < 4\,s$, we determine the minimum as the beginning of the avalanche, taking place at $t = 2.628 \pm 0.002\,s$. Thus, there is a significant time lag between the avalanche onset and the change in sign of $\overline{\lambda}(t)$.

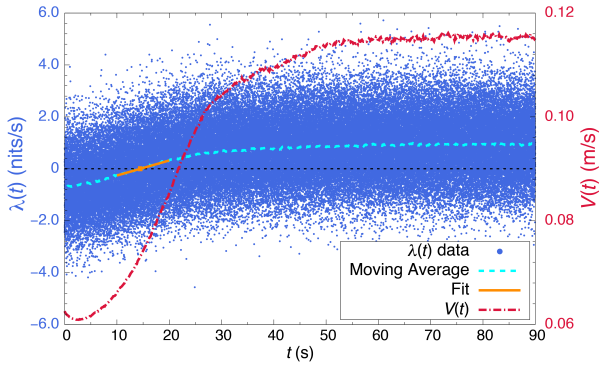

Figure 3. Chaotic behavior at avalanche onset. Scattered points represent the local Lyapunov exponent $\lambda(t)$ averaged over 70,000 independent runs. Even those data exhibit significant noise, which disappears in the moving average $\overline{\lambda}(t)$ (cf. main text). The latter exhibits a clear sign change (orange line segment) as the avalanche progresses, signaling the crossover from non-chaotic to chaotic behavior. To correlate this behavior with the dynamics of the system, the global speed $V(t)$ of all disks is shown as well (red dash–dotted line).

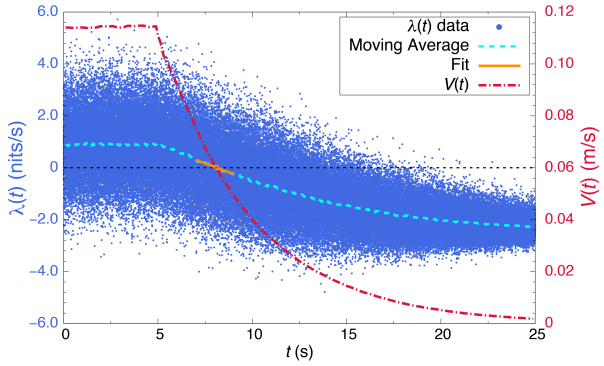

Figure 4. Dynamics at avalanche decay. Symbols are as described in Fig. 3. Following a continuous avalanche, avalanche decay starts at $t = 5\,s$, when the global speed $V(t)$ starts to decrease. This is accompanied by an immediate decrease in the moving average $\overline{\lambda}(t)$ of the first Lyapunov exponent, but a sign change in this exponent occurs only near $t = 8.13\,s$.

It is then natural to expect that the decay of the avalanche is accompanied by a second sign reversal of the local Lyapunov exponent. This is confirmed by the moving average $\overline{\lambda}(t)$ in Fig. 4. Adopting again a linear fit to $\lambda(t)$, now for $7\,s < t < 9\,s$, we determine the sign change at $t = 8.13 \pm 0.04\,s$. Since the decay of the avalanche is initiated exactly at $t = 5\,s$, we observe that the sign change of $\overline{\lambda}(t)$ again trails the change in state of the avalanche, although the lag is smaller than for the onset of the avalanche.

The time lag between the change in avalanche state and the change in sign of $\overline{\lambda}(t)$, both during avalanche onset and during avalanche decay, implies interesting conclusions regarding the dynamics of the rotating-drum system and its chaotic properties. On the one hand, it is noteworthy that even after the avalanche has started, the local dynamics of the system remain non-chaotic for some time. Conversely, even after the avalanche has started to decay, the local dynamics remain chaotic for a brief period. This is in contrast with the 2D shear cell [20], where the build-up of stress prior to an avalanche is accompanied by a gradual increase in the local exponent, which becomes positive well *before* the avalanche. On the other hand, despite the lag in the sign change, $\overline{\lambda}(t)$ shows an immediate response even for the rotating-drum system, starting to increase as soon as the avalanche is initiated (and likewise starting to decrease as soon as the avalanche decay begins). We remark that higher rotation speeds were found to decrease the time lag during avalanche onset [30]. Lastly, we note that the lack of static friction in our force model precludes direct comparison with an experimental study of the 2D rotating drum [22], where an immediate change in sign of $\lambda(t)$ was observed upon changes in the state of the avalanche. Due to experimental constraints, however, the authors in that study adopted different definitions of the Lyapunov vector for each avalanche regime, and we aim to overcome this drawback in future computational studies where we incorporate static friction.

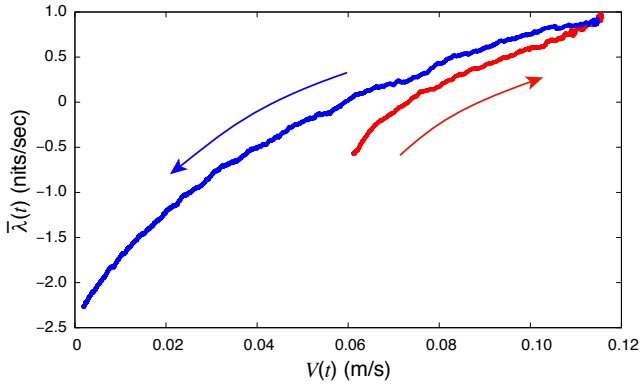

Figure 5. Correlation between the global speed $V(t)$ and the moving average $\overline{\lambda}(t)$ of the largest local Lyapunov exponent during avalanche onset (red) and decay (blue). Arrows indicate the direction of time evolution.

To elucidate the connection between the dynamics and chaotic properties of this system, we examine the global speed $V(t)$. Specifically, Fig. 5 shows how $\overline{\lambda}(t)$ has a monotonic dependence on $V(t)$ during both avalanche onset and decay. This is consistent with the strong spatiotemporal correlation between the velocity of each disk and the magnitude of the corresponding components of the Lyapunov vector in the 2D shear cell [20]. Here, we present a plausibility argument for this correlation by considering the dynamics of the individual particles in an avalanche. Indeed, it is known that the dynamics of a mobile disk bounded by a non-smooth (e.g., studded) cell is highly chaotic [31]. Similarly, we can think of each disk in the pile in Fig. 2(b) as bounded by a non-smooth cell comprised of its nearest

neighbors. If the majority of such cells are tight enough to effectively trap the contained disk in a near-stationary state, then there will be a lack of chaotic collisions and the overall dynamics of the system will be non-chaotic, consistent with the observation of negative Lyapunov exponents above the jamming transition [20]. On the other hand, if the system is in a state with many rattler disks that are frequently reflected by the "walls" of their respective cells, then we can expect more chaotic dynamics. In addition, the shifting and changing of the cells themselves would also contribute to increasingly divergent behavior [9]. In an avalanche, both conditions—rattler disks and shifting cells—are present. Particularly for a frictional system, the onset of an avalanche results in Reynolds dilatancy [32], leading to enlarged cells and more chaotic rattlers. Additionally, the mixing of the system during an avalanche leads to shifting and changing cells. This provides a heuristic basis for the close coupling of the system's global speed and its local Lyapunov exponent in both of the avalanche regimes.

IV SUMMARY AND CONCLUSION

We have examined chaotic dynamics near jamming and unjamming events of cylindrical disks in a rotating drum, motivated by recent experiments on a corresponding system and by computational work on disks in a 2D shear cell. Although we find that our system—unlike the shear cell—does not exhibit a positive local Lyapunov exponent prior to an unjamming event, we do confirm the strong correlation between global dynamics and chaotic properties. The largest local Lyapunov exponent shows an immediate response upon the onset or decay of an avalanche, and indeed becomes positive during an avalanche. We further confirm this correlation by demonstrating that this exponent has a monotonic dependence on the global speed of the disks and provide a plausibility argument for this observation.

We are currently extending these results to systematically examine the observed time lag between the onset of an avalanche and the sign change of the largest Lyapunov exponent, as a function of drum rotation speed. Moreover, in this future work we will incorporate static friction, which will make it possible to compare our findings to experimental studies of this system using photoelastic disks [22].

V ACKNOWLEDGMENTS

This research was supported by the U.S. National Science Foundation through Grant Nos. DMR-1121262 at the Materials Research Center of Northwestern University and DMR-1310211. We thank the Quest high-performance computing facility at Northwestern University for computational resources.

REFERENCES

[1] G. Metcalfe, T. Shinbrot, J. J. McCarthy and J. M. Ottino, Nature 374, 39 (1995).
[2] S. L. Conway, A. Lekhal, J. G. Khinast and B. J. Glasser, Chem. Eng. Sci. 60, 7091 (2005).
[3] D. E. Moran, J. Frankl. Inst. 199, 493 (1925).
[4] C. V. Givan, Eos, Trans. Am. Geophys. U. 15, 572 (1934).
[5] G. Baumann, I. M. Jánosi and D. E. Wolf, Phys. Rev. E 51, 1879 (1995).
[6] H. M. Jaeger, S. R. Nagel and R. P. Behringer, Rev. Mod. Phys. 68, 1259 (1996).
[7] A. Daerr and S. Douady, Nature 399, 241 (1999).
[8] I. S. Aranson and L. S. Tsimring, Rev. Mod. Phys. 78, 641 (2006).
[9] S. E. Cisar, J. M. Ottino and R. M. Lueptow, AIChE J 53, 1151 (2007).
[10] P. Richard, M. Nicodemi, R. Delannay, P. Ribière and D. Bideau, Nature Mater. 4, 121 (2005).
[11] H. M. Jaeger, Soft. Matt. 11, 12 (2015).
[12] S. C. Warren, O. Guney-Altay and B. A. Grzybowski, J. Phys. Chem. Lett. 3, 2103 (2012).
[13] T. Shinbrot, Nature Phys. 9, 263 (2013).
[14] S. Torquato, T. M. Truskett and P. G. Debenedetti, Phys. Rev. Lett. 84, 2064 (2000).
[15] A. Haji-Akbari, M. Engel, A. S. Keys, X. Zheng, R. G. Petschek, P. Palffy-Muhoray and S. C. Glotzer, Nature 462, 773 (2009).
[16] A. J. Liu and S. R. Nagel, Nature 396, 21 (1998).
[17] A. J. Liu and S. R. Nagel, Ann. Rev. Condens. Matt. Phys. 1, 347 (2010).
[18] D. Bi, J. Zhang, B. Chakraborty and R. P. Behringer, Nature 480, 355 (2011).
[19] M. E. Cates, J. P. Wittmer, J.-P. Bouchaud and P. Claudin, Phys. Rev. Lett. 81, 1841 (1998).
[20] E. J. Banigan, M. K. Illich, D. J. Stace-Naughton and D. A. Egolf, Nature Phys. 9, 288 (2013).
[21] C. S. O'Hern, S. A. Langer, A. J. Liu and S. R. Nagel, Phys. Rev. Lett. 88, 075507 (2002).
[22] Z. Wang and J. Zhang, Sci. Rep. 5, 8128 (2015).
[23] S. Schöllmann, Phys. Rev. E 59, 889 (1999).
[24] M. Lätzel, S. Luding and H. J. Herrmann, Gran. Matt. 2, 123 (2000).
[25] T. Pöschel and T. Schwager, *Computational Granular Dynamics: Models and Algorithms* (Springer, Berlin, 2005).
[26] J. Schäfer, S. Dippel and D. E. Wolf, J Phys I (France) 6, 5 (1996).
[27] M. P. Allen and D. J. Tildesley, *Computer Simulation of Liquids* (Clarendon, Oxford, 1987).
[28] A. H. Nayfeh and B. Balachandran, *Applied Nonlinear Dynamics: Analytical, Computational and Experimental Methods* (John Wiley, New York, 1995).
[29] E. Ott, *Chaos in Dynamical Systems* 2^{nd} edition (Cambridge University Press, Cambridge, 2002).
[30] H. Maghsoodi and E. Luijten (2016). In preparation.
[31] J. M. Haile, *Molecular Dynamics Simulation: Elementary Methods* (Wiley, New York, 1992).
[32] O. Pouliquen and N. Renaut, J Phys II (France) 6, 923 (1996).